THE JOURNAL OF BIOLOGICAL CHEMISTRY

Vol. 264, No. 18, Issue of June 25, pp. 10552-10566, 1989
Printed in U.S.A.

Folate Cycle Kinetics in Human Breast Cancer Cells*

(Received for publication, September 6, 1988)

Paul F. Morrison‡§ and Carmen J. Allegra¶

From the ‡Biomedical Engineering and Instrumentation Branch, Division of Research Services, National Institutes of Health and the ¶Clinical Pharmacology Branch, Division of Cancer Treatment, National Cancer Institute, National Institutes of Health, Bethesda, Maryland 20892

A mathematical description of polyglutamated folate kinetics for human breast carcinoma cells (MCF-7) has been formulated based upon experimental folate, methotrexate (MTX), purine, and pyrimidine pool sizes as well as reaction rate parameters obtained from intact MCF-7 cells and their enzyme isolates. The schema accounts for the interconversion of highly polyglutamated tetrahydrofolate, 5-methyl-FH_4, 5-10-CH_2FH_4, dihydrofolate (FH_2), 10-formyl-FH_4 (FFH_4), and 10-formyl-FH_2 (FFH_2), as well as formation and transport of the MTX polyglutamates. Inhibition mechanisms have been chosen to reproduce all observed non-, un-, and pure competition inhibition patterns. Steady state folate concentrations and thymidylate and purine synthesis rates in drug-free intact cells were used to determine normal folate V_{max} values. The resulting average-cell folate model, examined for its ability to predict folate pool behavior following exposure to 1 μM MTX over 21 h, agreed well with the experiment, including a relative preservation of the FFH_4 and CH_2FH_4 pools. The results depend strongly on thymidylate synthase (TS) reaction mechanism, especially the assumption that MTX di- and triglutamates inhibit TS synthesis as greatly in the intact cell as they do with purified enzyme. The effects of cell cycle dependence of TS and dihydrofolate reductase activities were also examined by introducing G- to S-phase activity ratios of these enzymes into the model. For activity ratios down to at least 5%, cell population averaged folate pools were only slightly affected, while CH_2FH_4 pools in S-phase cells were reduced to as little as 10% of control values. Significantly, these folate pool dynamics were indicated to arise from both direct inhibition by MTX polyglutamates as well as inhibition by elevated levels of polyglutamated FH_2 and FFH_2.

Folate kinetics have been the focus of intensive biochemical investigations for several decades. During this period, the major folate species and cofactors involved have been identified and connections between folate reactions and other pathways such as the *de novo* purine and pyrimidine synthetic routes have been ascertained. Quantitative description of folate kinetics has followed qualitative discovery, especially as a consequence of isolated enzyme kinetics experiments. Initial attempts to formulate kinetic models of the folate reactions were undertaken by Werkheiser (1971) and Werkheiser *et al.* (1973). More specialized kinetics were then introduced in the models of Jackson and Harrap (1973), Grindey *et al.* (1975), and White (1979). The most extensive folate model to date was formulated by Jackson (1980) and consisted of 63 reactions including those of the purine, pyrimidine, RNA, and DNA synthesis pathways. The effects of several drugs on metabolite pools and RNA/DNA synthesis rates were described by this model. This model was subsequently used to clarify the primary mode of action of antimetabolites, including methotrexate (MTX)[1] and 5-fluorouracil, the biochemical consequences of drug resistance, and the nature of drug-drug interactions (Jackson and Harrap, 1979; Jackson, 1986, 1987).

However, none of these models accounted for the polyglutamation of MTX or of the normal folates. Since the discovery of human erythrocyte MTX polyglutamation by Baugh *et al.* (1973), a large body of evidence has been collected showing that such polyglutamation occurs in a wide variety of mammalian cells (Jacobs *et al.* 1977; Whitehead *et al.*, 1975; Poser *et al.*, 1980; Rosenblatt *et al.*, 1978; Balinska *et al.*, 1982; Nimec and Galivan, 1983; Fry *et al.*, 1982; Jolivet *et al.*, 1982; Kennedy *et al.*, 1985) and that polyglutamates affect drug residence times in cells (Jolivet *et al.*, 1982; Kennedy *et al.*, 1983; Jolivet and Chabner, 1983). In addition, the degree of competitive inhibition between MTX and the normal folates for several enzymes depends strongly on the level of polyglutamation of both inhibitor and substrate. These polyglutamation effects alter our concept of the mode of action of MTX and therefore need to be included in a general description of folate kinetics. Furthermore, only recently have polyglutamated MTX and folate pool size measurements become available for the same human cell line from which enzymic kinetic parameters have been determined. The simultaneous availability of both types of experimental data thus set the stage for an improved, more internally self-consistent test of mathematical *versus* experimental kinetics.

Existing detailed models of folate kinetics have been developed for the description of murine cell lines and not for human lines. As a consequence, no human folate models have been available to test the quantitative self-consistency of known human reaction schemes and experimentally measured pool sizes and rate parameters. Accordingly, we have developed a

* The costs of publication of this article were defrayed in part by the payment of page charges. This article must therefore be hereby marked "*advertisement*" in accordance with 18 U.S.C. Section 1734 solely to indicate this fact.

§To whom correspondence should be addressed.

[1] The abbreviations used are: MTX, methotrexate; FH_4, tetrahydrofolate; FH_2, dihydrofolate; FFH_4, 10-formyl-FH_4; FFH_2, 10-formyl-FH_2; TS, thymidylate synthase; DHFR, dihydrofolate reductase; CH_2FH_4, 5,10-methylene-tetrahydrofolate; $MeFH_4$, 5-methyl-tetrahydrofolate; GAR, glycinamide ribonucleotide; FGAR, formylglycinamidine ribonucleotide; AICAR, aminoimidazole carboxamide ribonucleotide; FAICAR, formamidoimidazole carboxamide ribonucleotide; FA, FGAR amidotransferase; GT, glycinamide ribonucleotide transformylase; FDS, formyl dihydrofolate synthase; FTS, formyl tetrahydrofolate synthase; AT, AICAR transformylase; SH, serine hydroxymethyl transferase; MS, methionine synthase; MTD, methylene tetrahydrofolate dehydrogenase, MTR, methylene tetrahydrofolate reductase.

detailed model of polyglutamation-inclusive folate and MTX kinetics for the MCF-7 human breast cancer cell line, drawing on an extensive body of MCF-7 reaction rate and pool data collected in this laboratory (Jolivet *et al.*, 1982; Jolivet and Chabner, 1983; Allegra *et al.*, 1985, 1986; Schilsky *et al.*, 1981; Cowan and Jolivet, 1984; Clendeninn *et al.*, 1985; Baram *et al.*, 1987). The scope of this model is similar to the Jackson and Harrap (1973) model in that it includes some reactions of the purine pathway but generally neglects the pyrimidine and salvage pathways. It is more extensive, however, in that it includes MTX polyglutamation up through the pentaglutamate level, a more intricate pattern of inhibition arising from interactions of MTX polyglutamates and polyglutamated folate substrates, and the inclusion of 10-formyl-dihydrofolate. This human breast cancer folate model greatly expands our recently developed description of MTX polyglutamation-deglutamation kinetics (Morrison and Allegra, 1987) to include interactions with relevant folates and purines.

The development of a comprehensive folate model for human breast cancer cells is aimed at answering several questions. First, is our identification of the folate pathways and our quantification of them sufficiently complete to allow development of any reasonable kinetic model? Second, within experimental error, are the relative V_{max} and K_m values obtained from isolated enzyme studies consistent with the observed normal folate concentrations of drug-free MCF-7 cells? Third, are the presently discovered patterns of direct and indirect MTX inhibition, coupled with normal folate metabolism, capable of quantitatively reproducing the changes in population-averaged pool sizes induced by exposure to MTX? Fourth, after introducing cell cycle-dependent enzyme activities into the model, are these average pool sizes still reproduced and does indirect MTX inhibition still play a significant role relative to folate depletion? Quantitative inhibition of human folate enzymes has been largely characterized one enzyme at a time; our model tests whether the known constants of these enzymes are still capable of accounting for pool size alterations when all inhibitions occur simultaneously and are coupled through the entire folate cycle. It is especially important to see if the known polyglutamate interactions account for the observations that both cycle-averaged 5,10-methylene-tetrahydrofolate (CH_2FH_4) and 10-formyl-tetrahydrofolate (FFH_4) pools decline only slightly following exposure to 1 μM MTX (to 55 and 80% of control levels, respectively, after 2 h of exposure) (Allegra *et al.*, 1987). Relative stability of the cell-averaged CH_2FH_4 pool was not predicted by the earlier monoglutamate L1210 model (Jackson, 1980) where, instead, it declined precipitiously behind the dihydrofolate reductase block to just 3.5% of control after 2 h of exposure. The work reported here shows that these questions may generally be answered in the affirmative and thus that our set of MCF-7 data forms a quantitatively self-consistent description of folate kinetics in human breast cancer cells.

DEVELOPMENT OF THE KINETIC MODEL

The Folate Reactions—The description of folate reactions may be considered at either the cellular or cell population level. Our approach is to first describe folate metabolism in terms of reactions operating at the cellular level for cells in any phase of the cell cycle. These reactions, associated mechanisms and inhibitions, and differential mass balances are presented in this section. Population level effects are described under "Results" in the context of parameterization of the model to MCF-7 cells.

The folate reactions that form the basis of the model are shown in Fig. 1. The following three overall reaction loops have been included: (i) the production of 5-methyl-tetrahydrofolate ($MeFH_4$) from CH_2FH_4 and its return via tetrahydrofolate (FH_4); (ii) the formation of FFH_4 from either CH_2FH_4 or FH_4, reactions providing the folate cofactor needed for purine synthesis; and (iii) the production of thymidylate from deoxyuridylate and CH_2FH_4 and subsequent reduction of FH_2 by dihydrofolate reductase (DHFR) to FH_4. Purine synthesis includes the formylation of both glycinamide ribonucleotide (GAR → FGAR) and aminoimidazole carboxamide ribonucleotide (AICAR → FAICAR) as well as the connecting reaction between FGAR and AICAR involving FGAR amidotransferase (FA) (Jackson, 1980). All reactions are enzymatically driven (Table I) except the addition of the methylene group to FH_4 via formaldehyde.

The selection of these reactions follows in great part from the folate cycle descriptions of Blakeley (1969) and Rader and Huennekens (1973) as well as by the choice of reactions included in the folate kinetic models of Jackson and Harrap (1973) and Jackson (1980). However, certain modifications of these earlier schemes were made, both to simplify and to account for recent observations of the behavior of MCF-7 breast cancer cells in culture.

The first of these changes was to consider intracellular serine and glycine concentrations constant because of their rapid resupply from the RPMI 1640 medium via the amino acid transport system. Earlier models allowed serine to be formed by its normal biosynthetic route from the 3-phosphoglyceric acid intermediate of glycolysis; glycine

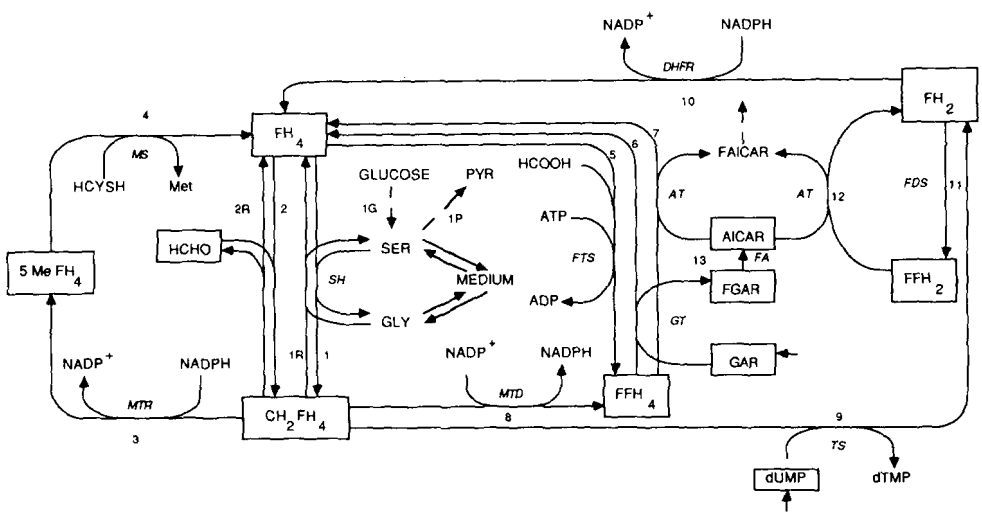

FIG. 1. **Schematic of the folate cycle.** Abbreviations appear in text. *Boxes* identify species for which differential mass balances have been constructed in the model. Numbers correspond to the reaction numbers in Tables I–III.

TABLE I
Folate mechanisms and inhibitions

Reaction[a] (no./enzyme)	Mechanism	Inhibitions[b]
1 Serine hydroxymethyl transferase	RORE[c]	None
3 Methylene tetrahydrofolate reductase	RORE	MTX_n, FH_2 (competitive *vs.* folate)(noncompetitive *vs.* NADPH)
4 Methionine synthase	RORE	None
5 Formyl tetrahydrofolate synthase	RORE (3 substrates)	None
6 GAR transformylase	RORE	MTX_n, FH_2, FFH_2 (competitive)
7,12 AICAR transformylase	RORE	MTX_n, FH_2 (competitive)
8 Methylene tetrahydrofolate dehydrogenase	RORE	None
9 Thymidylate synthase	Ordered (dUMP, folate)	MTX_n, FH_2, FFH_2, (uncompetitive: MTX_1) (noncompetitive: MTX_{2-5}) (competitive: FH_2; FFH_2)
10 Dihydrofolate reductase	Random order	MTX_n
11 Formyl dihydrofolate synthase	First Order (in FH_2)	None
13 FGAR amidotransferase	RORE	None
— Folylpolyglutamate synthase	First order (in MTX_n)	None[d]
— Folylpolyglutamate hydrolase	First order (in MTX_n)	None[d]
— Methyltetrahydrofolate permease		
Influx	Michaelis	None
Efflux	First order	None[e]

[a] Reaction catalyzed by enzyme is identified by reaction number in Fig. 1; last three enzymes catalyze MTX_n polyglutamation-deglutamation and transport processes not shown in Fig 1.
[b] Against normal folate pentaglutamate substrates unless denoted otherwise.
[c] Random order rapid equilibrium.
[d] Inhibition by other MTX polyglutamates negligible for our dose and exposure range.
[e] MTX1 inhibition characteristic of a 1 μM dose may be implicit in the first order rate constant.

was then formed from serine by the action of serine hydroxymethyltransferase (*reaction 1* in Fig. 1). These earlier models also allowed for the reverse process encountered with oxidative degradation of amino acids, hence the reverse glycine to serine reaction and the serine dehydratase degradation of serine to pyruvate (*reaction 1P*). While all these reactions are operative in MCF-7 cells, their role in establishing serine and glycine concentrations is greatly reduced when these cells are grown in media supplemented with amino acids. Furthermore, with glucose present in the medium, oxidative degradation of amino acids is not required for energy production, and fluxes through these pathways may be expected to be small. Because we have applied our folate model to cells growing in supplemented media, we therefore have kept serine and glycine constant at their intracellular values (as indicated by the exchange with medium in Fig. 1) and have omitted reactions 1G and 1P.

The second alteration from previous folate schemes was to omit specific representation of N^5,N^{10}-methenyl-tetrahydrofolate as a folate intermediate in the conversion of CH_2FH_4 to FFH_4. In Jackson (1980), the methenyl compound was shown as the primary substrate for glycinamide ribonucleotide transformylase (GT). However, the methenyl compound interconverts rapidly with FFH_4 and, at intracellular pH, the balance of this interconversion lies strongly to FFH_4. In addition, experiments performed by Smith *et al.* (1981) clearly illustrate that FFH_4 and not the methenyl compound is the primary substrate for GT.

Reactions that are unique to our model include those accounting for the synthesis and loss of 10-formyl-dihydrofolate (FFH_2) following long term exposure of MCF-7 cells to MTX (Allegra *et al.*, 1986). This compound has been shown to be produced from FH_2, formate, and ATP by formyl dihydrofolate synthase (FDS), an enzyme similar to but distinct from formyl tetrahydrofolate synthase (FTS) (Drake *et al.*, 1987a). FFH_2 is both substrate and inhibitor depending upon enzyme (Baram *et al.*, 1987). It serves as a substrate of AICAR transformylase (AT) (*reaction 12*) but as an inhibitor of both TS and GT (*reactions 9* and *6*). Other reactions that have been added to our folate model (not shown in Fig. 1) include those describing polyglutamation-deglutamation of MTX and transport of the various MTX polyglutamate forms across the cell membrane (Morrison and Allegra, 1987). Normal folate species and FFH_2 are assumed to be highly (approximately penta-) polyglutamated; hence no reactions describing polyglutamation-deglutamation of these species are included in our model. We have also allowed for the induction of DHFR synthesis in the presence of MTX (Jolivet and Chabner, 1983; Morrison and Allegra, 1987).

Folate Reaction Mechanisms and Inhibitors—Enzyme reaction mechanisms for the folate model are summarized in Table I. Enzymes catalyzing the reactions in Fig. 1 are identified by reaction number; the enzymes responsible for polyglutamation, deglutamation, and transport appear as the last three unnumbered entries in the table. The random order rapid equilibrium (RORE) mechanism has been used most frequently in our model and, following Jackson (1980), has been applied to SH, MS, FTS, GT, AT, MTD, and FA. All reactions where RORE has been used are assumed to be bisubstrate except for reaction 5 (FTS) where three substrates (ATP, formate, FH_4) are involved. RORE substrates identical to those of Jackson (1980) (other than in polyglutamation level) are employed except at MS where we have neglected explicit representation of the B_{12} cofactor (instead lumping this third substrate in with the V_{max}), and at GT where FFH_4 rather than N^5,N^{10}-methenyl-FH_4 is considered to be the primary substrate. Binding of the normal FH_2 and NADPH substrates to dihydrofolate reductase is also considered to occur in random order, although no significant quantitative difference in rate would occur if NADPH were assumed to bind first. However, because of the extremely tight binding of the MTX_n inhibitors and relatively large amount of DHFR present, substrate and inhibitor concentrations are not assumed to be in great excess of total enzyme concentration and

complete binding equilibria specifically accounting for bound, free, and total substrate and inhibitor concentrations are retained throughout. FH_2 and NADPH are assumed to be at steady state with free enzyme but inhibitor binding is treated kinetically (Jackson, 1980; Morrison and Allegra, 1987).

The reaction at methylene tetrahydrofolate reductase (MTR) can be described mechanistically, as folate glutamate chain length increases, either by a ping-pong giving way to an ordered sequential process or by an ordered bi-bi giving way to a rapid equilibrium random process (Matthews and Baugh, 1980). The long chain length mechanisms require that folate chain lengths exceed three, a situation present in intact MCF-7 cells where the pentaglutamate level is easily reached (Jolivet *et al.*, 1982; Kennedy *et al.*, 1985). Our model employs the rapid equilibrium random order mechanism.

The reaction at TS is described as an ordered process where it is assumed that dUMP first binds to enzyme followed by the folate cofactor (Danenberg and Danenberg, 1978). Other mechanisms have been proposed in which reverse or random ordering have been proposed (Reyes and Heidelberger, 1965; Lorenson *et al.*, 1967; Santi *et al.*, 1976). However Galivan *et al.* (1976) investigated polyglutamated CH_2FH_4 binding and found that while polyglutamation enhanced binding strength, the presence of dUMP enhanced it more, suggesting that dUMP may in fact bind first. Our choice of mechanism reflects this ordering. However, we have also found that, given the substrate concentrations and binding constants for the MCF-7 system, there is very little quantitative difference in rate between the nucleotide/folate-ordered mechanism and a random mechanism.

Reaction mechanisms for the folylpolyglutamate synthase and hydrolase enzymes are pseudo-first order in MTX polyglutamate concentration and have been discussed previously (Morrison and Allegra, 1987). These enzymes are assumed to be in equilibrium with a constant concentration of glutamate. In addition, while they may saturate with folate or MTX substrate at some level, the folate and drug concentrations encountered in the entire set of experimental MCF-7 data with which we have dealt are sufficiently low that negligible saturation by these species need be considered. We estimate that neglect of saturation after 20 h of exposure to 1 μM MTX leads to an error of no more than 10–20% in polyglutamation-deglutamation reaction rates, a percentage that is less than the fitting error in rate constant determination (Morrison and Allegra, 1987). Likewise, efflux of MTX polyglutamate is treated as a pseudo-first order process. This treatment is more approximate than with the synthase/hydrolase enzymes since intracellular parent MTX may begin to saturate the efflux carrier at extracellular concentrations of 1 μM or higher, and $MeFH_4$ pentaglutamate might possibly act as inhibitor of the carrier. However, each of these effects is unlikely to exceed 30% if the efflux Michaelis constant is 4 μM or more and, most importantly, much of this error has already been taken into account empirically over the dose range of 0.2–10 μM as a consequence of fitting first order efflux constants to observed MTXn pool levels (Morrison and Allegra, 1987). Because we are concerned with folate pool variation following exposure to 1 μM MTX in this report, we are within the 0.2–10 μM empirical range, and the first order constants determined previously remain applicable.

Influx of MTX polyglutamates, on the other hand, is described by a saturable Michaelis mechanism (Morrison and Allegra, 1987). Because we only consider MCF-7 cells growing in a relatively large volume of culture medium, we have restricted the description of influx to MTX monoglutamate. Insufficient higher MTX polyglutamates exit the cell to pose any need for description of reentry.

The various patterns of inhibition operating in the MCF-7 folate model are also summarized in Table I. MTX polyglutamates (MTXn) and FH_2 (polyglutamate) are inhibitors at MTR, TS, GT, and AT (Allegra *et al.*, 1985, 1985b, 1985c, 1986, 1987a, 1987b; Baram *et al.*, 1987). In addition, the MTX polyglutamates inhibit DHFR and FFH_2 inhibits TS and GT (Baram *et al.*, 1987). The patterns of inhibition at MTR are obtained by allowing the FH_2 and MTX inhibitors to bind only to free enzyme or to enzyme with the NADPH substrate attached, *i.e.* these inhibitors compete with CH_2FH_4 polyglutamate for its binding site. The noncompetitive inhibition observed with variable NADPH substrate becomes pure noncompetitive if these inhibitors bind to the two enzyme forms with identical binding constants. Inhibition patterns at TS are complex, with competitive, uncompetitive, and noncompetitive patterns all obtained with variable folate substrate depending on specific inhibitor considered (Allegra *et al.*, 1985). Our model accounts for these patterns by extending the mechanism of Allegra *et al.* (1985) to include the dUMP-bound enzyme forms. In particular, three binding sites are assumed, one for dUMP, one for CH_2FH_4 as well as FFH_2 inhibitor, and another to which MTXn and FH_2 inhibitors may bind. Furthermore, dUMP must bind before either CH_2FH_4 or FFH_2 binds and one of these latter must bind before MTX monoglutamate may attach to its site. Higher MTX polyglutamates and FH_2 may bind to enzyme whether or not dUMP, CH_2FH_4, or FFH_2 have bound previously. Such a mechanism leads to 14 enzyme complexes (including free enzyme), and reproduces the inhibition patterns of Table I observed when dUMP was in great excess.

Inhibition of DHFR by MTX polyglutamates has been described previously (Morrison and Allegra, 1987). In brief, a reversible tight binding mechanism has been employed in which FH_2 and NADPH achieve instanteous equilibrium with enzyme, MTX polyglutamates attach at the FH_2-binding site, and the drug binding reactions are slow relative to those of FH_2. MTXn /DHFR association rate constants (k_n) depend on polyglutamate chain length, while the dissociation constants (k_{off}) do not (Morrison and Allegra, 1987; Clendeninn *et al.*, 1985). DHFR-bound MTXn (y_n) is thus given by

$$\frac{dy_n}{dt} = k_n D_f x_n - k_{off} y_n \qquad n \geq 1 \tag{1}$$

where D_f is the MTXn-free DHFR concentration (*i.e.* the binary NADPH/native-DHFR complex concentration given that the enzyme is saturated with NADPH) and x_n is the free MTXn-glutamate. (These terms also appear in the expressions for dx_n/dt, along with terms describing cellular influx and efflux and glutamation-deglutamation.) An expression for the MTXn-free DHFR concentration, D_f, is given below.

Inhibition of DHFR by MTXn has one additional component, an increase of the total enzyme content in a population of cells exposed to the drug. Following the Domin *et al.* (1982) attribution of this enzyme increase to enhanced synthesis, total DHFR concentration was thus described as resulting from a balance between zero-order synthesis and first order degradation, where the normal synthesis rate (k_{00}) took on an increased value in the presence of drug (k_0). Drawing on experimental observations of this induction in human breast cancer cells (Jolivet and Chabner, 1983), the synthesis/degradation reactions were balanced in our model so that DHFR enzyme content doubled during 24 h of exposure to MTX (Morrison and Allegra, 1987).

The inhibition of both GT and AT by MTXn and FH_2 (Table I) was modeled as simple competitive inhibition of binding of the normal FFH_4 substrate. This competitive mechanism was also used to describe the inhibition of GT by FFH_2 (Baram *et al.* 1987).

The Folate Cycle Model—The folate cycle model for any phase cell consists of 21 differential mass balances formulated for the 11 boxed species of Fig. 1 plus 10 MTX species, five of these being the free MTXn species up through the pentaglutamate level and the other five being their DHFR-bound counterparts. In addition, the model allows for a mass balance on DHFR synthesis and degradation.

The balances for free methotrexate n-glutamate (x_n) are (Morrison and Allegra, 1987)

$$\frac{dx_n}{dt} = -L_{n,n+1}x_n + L_{n-1,n}x_{n-1} - L_{n,n-1}x_n + L_{n+1,n}x_{n+1} - L_n x_n - k_n D_f x_n + k_{off} y_n \qquad n \geq 2 \tag{2a}$$

$$\frac{dx_1}{dt} = L_I x_{10} - L_1 x_1 - k_1 D_f x_1 + k_{off} y_1 - L_{12} x_1 + L_{21} x_2 \tag{2b}$$

where the $L_{n,n'}$ coefficients are rate constants for glutamation and deglutamation, L_n are efflux rate constants, k_n are association rate constants of MTXn with DHFR, k_{off} is the dissociation rate constant, D_f is the MTXn-free native DHFR-NADPH complex, x_{10} is the concentration of MTX1 in the culture medium, and L_I is the influx rate coefficient

$$L_I = V/(K_t + x_{10}) \tag{3}$$

The balances for bound methotrexate n-polyglutamate appear as Equation 1. An expression for the DHFR concentration unbound to MTXn (D_f) can be obtained from the instanteous mass balance on this enzyme,

$$D = D_f + (FH_2)D_f/K_{FH_2} + \sum_1^5 y_n \tag{4}$$

where the total DHFR (D) is the sum of free, FH_2-bound, and MTXn-

bound forms, and equilibrium between free DHFR (saturated with NADPH) and free FH_2 has been assumed. D_f derived from this expression depends on D, free FH_2, and the y_n. Differential mass balances provide relationships for D (below) and the y_n, but since the dihydrofolate differential mass balance is more easily written for total (FH_2^T) than free compound, FH_2 in Equation 4 must be replaced by the FH_2^T given by the instanteous mass balance for dihydrofolate

$$FH_2^T = FH_2 + FH_2(D_f)/K_{FH_2} \tag{5}$$

The resulting quadratic equation in D_f may then be solved for D_f, this variable emerging as the positive root solution. As shown in Morrison and Allegra (1987), the total DHFR content of the cell is given by

$$D = D_0[\alpha + (1 - \alpha)\exp(-k_d t)] \tag{6}$$

where D_0 is the normal cellular DHFR concentration, k_d is the degradation rate constant of DHFR, α is the ratio of DHFR synthesis rates in the absence and presence of MTX (= 1 if no drug is present), and t is the time over which enzyme is drug bound. For this equation to apply, drug must be present at levels that bind the great bulk of DHFR, and the drug must be present continuously over the simulation period.

The differential mass balances for the folate, pyrimidine, and purine compounds follow from the reaction fluxes depicted in Fig. 1. If each reaction is denoted by r_i, where i is the reaction number in Fig. 1, then

$$\frac{dFH_2^T}{dt} = \sum_{9,12} r_i - \sum_{10,11} r_i \tag{7.1}$$

$$\frac{dFH_4}{dt} = \sum_{1R,2R,4,6,7,10} r_i - \sum_{1,2,5} r_i \tag{7.2}$$

$$\frac{d(CH_2FH_4)}{dt} = \sum_{1,2} r_i - \sum_{1R,2R,3,8,9} r_i \tag{7.3}$$

$$\frac{dMeFH_4}{dt} = r_3 - r_4 \tag{7.4}$$

$$\frac{dFFH_4}{dt} = \sum_{5,8} r_i - \sum_{6,7} r_i \tag{7.5}$$

$$\frac{dFFH_2}{dt} = r_{11} - r_{12} \tag{7.6}$$

$$\frac{dHCHO}{dt} = r_{2R} - r_2 \tag{7.7}$$

$$\frac{d(dUMP)}{dt} = U_0 - r_9 \tag{7.8}$$

$$\frac{dGAR}{dt} = G_0 - r_6 \tag{7.9}$$

$$\frac{dFGAR}{dt} = r_6 - r_{13} \tag{7.10}$$

$$\frac{dAICAR}{dt} = r_{13} - r_7 - r_{12} \tag{7.11}$$

where U_0 and G_0 are the steady state synthesis rates of thymidylate and GAR synthesis in drug-free MCF-7 cells. Three of these r_i values are linear or ordinary bimolecular, *i.e.* $r_{11} = k_{FDS}(FH_2)$, $r_{2R} = h_i(CH_2FH_4)$, and $r_2 = h_p(FH_4)(HCHO)$. Linearity is assumed for r_{11} because the Michaelis constants for the FDS enzyme have not yet been ascertained. The simple expressions for r_2 and r_{2R} stem from the nonenzymatic character of the HCHO reaction. The reduction rate of FH_2 is given by the product of the DHFR/NADPH/FH_2 ternary complex concentration with the rate constant, k, of its breakdown, *i.e.*

$$r_{10} = k(FH_2^T - FH_2) \tag{8}$$

where the ternary complex is expressed as the difference between total and free FH_2. FH_2^T is determined by Equation 7.1 and FH_2 by Equation 5 after evaluating D_f in terms of the principal variables, D (Equation 4), y_n (Equation 1), and FH_2^T. The reaction for FTS, r_5, is the only trisubstrate reaction in the model and is described by the random order rapid equilibrium relationship (Jackson and Harrap, 1973)

$$r_5 = \frac{V_{FTS}}{(1 + K_{FH_4}/FH_4)\ (1 + K_{ATP}/ATP)\ (1 + K_{formate}/Formate)} \tag{9}$$

All other reactions are described by the generalized bisubstrate reaction term with inhibition

$$r_i = \frac{V_i S_{1i} S_{2i}}{K_{1i}K_{2i}\beta_i + K_{1i}S_{2i}\gamma_i + K_{2i}S_{1i}\delta_i + S_{1i}S_{2i}\epsilon_i} \tag{10}$$

where substrate 1 is the folate species, substrate S_{1i} pairs with K_{1i}, and algebraic forms for β_i, γ_i, δ_i, and ϵ_i are given for each enzyme in Table II. These forms reproduce the inhibition patterns listed in Table I.

The choice of a constant production rate of dUMP and GAR (U_0 and G_0) has been adopted from Jackson and Harrap (1973), although the concentrations of these species are regulated and certainly never attain the infinite levels upon continued drug exposure that are allowed by their differential mass balances. However, this is of little consequence for thymidylate and FGAR production because the TS and GT enzymes rapidly saturate with substrate upon MTX exposure, such saturation levels apparently occurring far below the maximal levels imposed by regulatory mechanism (Jackson and Harrap, 1973; Myers *et al.*, 1975). Thus, in the continued presence of drug, folate, pyrimidine, and purine pool sizes should be determined without introduction of more extensive pyrimidine and purine pathways. (This differs from Jackson and Harrap (1973) in which their consideration of a second drug product, FdUMP and its competition with dUMP for TS, forced them to place a ceiling on the allowable dUMP concentration.)

Numerical Methods—The folate model consists of the 21 ordinary, nonlinear, stiff differential equations of Equations 1, 2, and 7.1–7.11 which depend, in turn, on the expression for D_f obtained from Equations 4 and 5, the expression for total DHFR from Equation 6, and reaction term definitions of Equations 8–10. In addition, initial values for each variable are required as well as numerical values for each parameter appearing in these equations. The parameter values are discussed below. The set of differential equations were coded in FORTRAN and solved on a VAX 11/750 using the Gear integrator of the IMSL package (IMSL, 1982). A 50-h simulation requires about 50 s run time, given present input/output. A similar speed version has also been run on the Mac II with graphics output to Cricketgraph.

RESULTS

The set of reactions and inhibitions comprising the folate model have been largely quantified by *in vitro* experiments on whole cells and cell extracts obtained from nonsynchronized populations of human MCF-7 breast cancer cells. We therefore examined the system of reactions and associated parameters for completeness and self-consistency by comparing model predictions of population-averaged folate pool sizes, pyrimidine, and purine synthesis rates against experimental determinations of these quantities. The steps needed for this examination required that (*a*) available experimental parameters be identified and tabulated, (*b*) missing parameters be determined from fits to steady state folate pool concentrations in drug-free cells, and (*c*) the fully parameterized model be examined for its ability to predict experimental folate pool dynamics, during continuous drug exposure.

Because a model, based upon a population of cell cycle-independent cells, captures most folate dynamics, we first describe parameterization and simulation in terms of such a population. We then conclude this section with a description of the impact of cycle-dependent enzyme activities on parameterization and the ability to account for experimental data.

Parameterization—The reactions and inhibitions of our methotrexate-folate cycle system depend on 95 independent parameters (although not all contribute uniquely to folate dynamics; see "Discussion"). These parameters are summarized in Tables III and IV where, for convenience, both experimental and final (cycle-independent) model values are

TABLE II

Generalized bisubstrate reaction coefficients

For use with Equation 10 with substrate 1 identified as the folate species. x_n is defined as the free concentration of MTX_n. FH_2 and FFH_2 refer to the free pentaglutamated dihydrofolate and formyl dihydrofolate forms.

Enzyme (reaction no. i)		β_i	γ_i	δ_i	ϵ_i
SH	(1)	1	1	1	1
	(1R)	1	1	1	1
MTR	(3)	$1 + \sum_1^5 \frac{x_n}{K_3^{MTX_n}} + \frac{FH_2}{K_3^{FH_2}}$	β_3	1	1
MS	(4)	1	1	1	1
GT	(6)	$1 + \sum_1^5 \frac{x_n}{K_6^{MTX_n}} + \frac{FH_2}{K_6^{FH_2}} + \frac{FFH_2}{K_6^{FFH_2}}$	β_6	1	1
AT	(7)	$1 + \sum_1^5 \frac{x_n}{K_7^{MTX_n}} + \frac{FH_2}{K_7^{FH_2}} + \frac{FFH_2}{K_7^{FFH_2}}$	β_7	1	1
	(12)	$1 + \sum_1^5 \frac{x_n}{K_7^{MTX_n}} + \frac{FH_2}{K_7^{FH_2}} + \frac{FFH_4}{K_7^{FFH_4}}$	β_{12}	1	1
MTD	(8)	1	1	1	1
TS	(9)	$1 + \sum_2^5 \frac{x_n}{K_9^{MTX_n}} + \frac{FH_2}{K_9^{FH_2}}$	$\beta_9 + \frac{FFH_2}{K_9^{FFH_2}} \epsilon_9$	0	$\beta_9 + \frac{x_1}{K_9^{MTX1}}$
FA	(13)	1	1	1	1

given. Table III lists the Michaelis, maximum velocity, and inhibition constants for the bisubstrate reactions (Table II and Equation 10) as well as constants required for the FDS and FTS reactions (r_{11} and r_5) and the binding of FH_2 and MTX to DHFR. Table IV lists all other parameters.

A review of the experimental data in these tables shows that the great majority of these values are available from experiments performed on the MCF-7 cell line, thus indicating that we could maintain a high degree of cell-line consistency during the construction of our model. Principal exceptions to the MCF-7 source occur in the set of second-substrate non-folate Michaelis constants (K_{2i} of Table III) where values at SH, AT, and TS were estimated from pig liver, chicken liver, and human AML sources and values at MTR, MS, GT, FA, and MTD were taken from the Jackson (1980) model which drew on L1210, L5178Y, and chicken liver sources. Of the folate-binding constants, only those for pentaglutamyl FH_2 inhibition of MTR, FH_4 binding at SH, and CH_2FH_4 at MTD were non-MCF-7 (pig liver). All 50 remaining substrate and inhibition constants in Table III (including the association/dissociation constants for FH_2 at DHFR) are from the MCF-7 cell line. (Constants for reverse SH and FTS, although non-MCF-7, are unimportant since these enzymes are associated with very small fluxes in the cycle.) Likewise, all of the 25 cell-related values in Table IV have been derived from or shown to be consistent with MCF-7 data (Morrison and Allegra, 1987).

Polyglutamation plays an important role in the MCF-7 breast cancer line. The inhibition constants at MTR, TS, AT, and GT, the association/dissociation constants at DHFR, and the polyglutamation and efflux constants in Table IV account for both the direct and indirect effects of MTX polyglutamation. In addition, the inhibition constants included in Table III are those obtained from experiments in which pentaglutamated rather than monoglutamated substrates were inhibited. This is a necessary consideration since the polyglutamyl inhibitor constants reported for MTR, AT, and GT are apparent constants that depend on the chain length of the normal substrate (Matthews and Baugh, 1980; Allegra *et al.* 1985b). Were short chain lengths, uncharacteristic of cellular folates, used for the substrates, the strength of inhibition of these enzymes by MTX, FH_2, and FFH_2 would be greatly overestimated, generally by 10-fold.

The goal of the folate model is to have it describe the folate biochemistry of an intact human breast cancer cell. Hence, our approach to parameterization has been to include in the the model those experimental constants that are taken directly from whole cells as well as those obtained from cell isolates that are likely to have been little affected by the isolation procedure. Because the enzymes of the folate system are cytosolic, it appeared reasonable to assume that substrate and inhibitor constants determined on isolated enzymes were good approximations to their values in the intact cell since the steric factors and bond energies underlying these parameter values should not be altered by the presence or absence of cellular membranes. Activity differences, due to larger protein concentrations in the cytosol, remain as affecting factors, but these are not expected to exceed parameter reproducibility error. However, there is less reason to assume *a priori* that isolated enzyme V_{max} values can be carried over to the intact cell and we have not generally done so (see next section). These V_{max} estimates may be subject to substantial experimental error such as undetected redox destruction of compound and incompletely determined purification level.

Steady State Drug-free Folate Model—While substrate and inhibitor binding constants have been taken largely from isolated enzyme experiments, most V_{max} values have been determined from steady state folate pool concentrations measured in drug-free MCF-7 cells. Allegra *et al.* (1986) found that the steady state percentages of the total folate concentration in MCF-7 cells were: FH_4, 14.8%; CH_2FH_4, 7.8%; $MeFH_4$, 49.6%; FFH_4, 27.8%; and FH_2, not detectable. Total intracellular folate concentration, exclusive of folic acid and 5-formyl-FH_4 and allowing for assay recovery, was 3.36 μM. These steady state levels are described by the model Equations 7.1–7.5 with the time derivatives set equal to zero. Although there are five such algebraic equations, only three are directly useful for determining V_{max} values since one is linearly dependent

TABLE III

Enzyme kinetic parameters

Units: K in μM, V in μM/hr. Table of values for cell cycle-independent model; in the cycle-dependent model, TS and DHFR activities (V_9 and k) are scaled up by 3.16 for S-phase cells and down by 0.158 for G-phase cells, while k_{FDS} becomes 60 h^{-1}. Reaction numbers are from Fig. 1. NA = not available. Boldface numbers display largest differences between model and isolated enzyme parameter values. Italics identify non-MCF-7 constants. J denotes parameter values estimated from the Jackson, 1980, model. All other listed constants have been measured in this laboratory.

Enzyme	r_i		K_{1i}	K_{2i}	V_i	K_i^{FH2}	K_i^{FFH2}	K_{12}^{FFH4}	$K_i^{MTX_n}$ (n = 1,5)
SH	(1)	Model	1.7 (FH_4)	210 (Ser)	**18,330**				
		Expt.	*1.7*[a]	*210*[a]	7,200[b]				
	(1R)	Model	3,200 (CH_2FH_4)	10^4 (Gly)	12.2×10^6				
		Expt.	*J*	*J*	*J*				
MTR	(3)	Model	50 (CH_2FH_4)	50 (NADPH)	**224.8**	**0.40**			59.0, 21.3, 7.68, 2.77, 1.00
		Expt.	50[c]	*J*	*420.0*[b]	*0.04*[d]			59.0, 21.3, 7.68, 277, 1.00[c]
MS	(4)	Model	125 ($MeFH_4$)	2,900 (HCYSH)	**22,600**				
		Expt.	125[e]	*J*	12,100[e]				
GT	(6)	Model	4.9 (FFH_4)	52 (GAR)	**4,126**	**5.0**	**1.0**		84.0, 60.0, 43.0, 31.0, 22.0
		Expt.	4.9[f]	*J*	9,070[f]	8.7[f]	2.0[f]		84.0, 60.0, 43.0, 31.0, 22.0[b]
AT	(7)	Model	5.5 (FFH_4)	24 (AICAR)	**31,675**	2.89	5.3		40.0, 31.5, 2.33, 3.61, 5.89
		Expt.	5.5[f]	*24*[g]	63,350[h]	2.89[h]	5.3[f]		40.0, 31.5, 2.33, 3.61, 5.89[b]
	(12)	Model	5.3 (FFH_2)	24 (AICAR)	**9,503**	2.89		5.5	40.0, 31.5, 2.33, 3.61, 5.89
		Expt.	5.3[f]	*24*[g]	$\sim V_7$[f]	2.89[h]		5.5[f]	40.0, 31.5, 2.33, 3.61, 5.89[b]
MTD	(8)	Model	3.0 (CH_2FH4)	21.8 ($NADP^+$)	68,500				
		Expt.	*3.0*[i]	*J*	NA				
TS	(9)	Model	2.5 (CH_2FH4)	1.8 (dUMP)	**58**	3.0	1.6		13.0, **0.08, 0.07, .065,** .047
		Expt.	2.5[f]	*1.8*[j]	39.7[f]	3.9[f]	1.6[f]		13.0, 0.17, 0.14, 0.130, 0.047[b]
FA	(13)	Model	100 (Gln)	100 (FGAR)	4656				
		Expt.	*J*	*J*	*J*				

			K_{FH4}	K_{ATP}	$K_{formate}$	V_5
FTS	(5)	Model	230	56	1,600	3,600
		Expt.	*230*[k]	*56*[k]	*1,600*[k]	*J*

			k_{FDS} (h^{-1})
FDS	(11)	Model	65[l]
		Expt.	—

			K_{FH2}	k (ternary rate constant, h^{-1})	k_{off} (h^{-1})	k_n(n = 1,5)($\mu M^{-1}hr^{-1} \times 10^{-6}$)
DHFR	(10)	Model	0.32	2,109.4	0.42	0.231, 0.443, 0.851, 1.63, 3.14
		Expt.	0.32[m]	2,109.4[n]	0.42[m]	0.231, 0.443, 0.851, 1.63, 3.14[m]

[a] Matthews *et al.*, 1982, pig liver. [b] Allegra *et al.*, 1985c. [c] C. J. Allegra, unpublished data. [d] Matthews and Baugh, 1980, pig liver. [e] J. Jolivet, unpublished data. [f] Baram *et al.*, 1988. [g] Baggot and Krumdieck, 1979, chicken liver. [h] Allegra *et al.*, 1985b. [i] MacKenzie and Baugh, 1980, pig liver. [j] Dolnick and Cheng, 1977, human AML cells. [k] Tan *et al.*, 1977, pig liver. [l] Model value reproduces experimental FFH_2/FH_z ratio following 21 h of 1 μM MTX exposure. [m] Clendinnen *et al.*, 1985. [n] Drake *et al.*, 1987b.

through conservation of mass, and another one is effectively linearly dependent as a consequence of the near-zero FH_2 concentration. Thus, three of these steady state equations (Equations 7.3–7.5) were used to determine three V_{max} quantities accounting for the observed steady state folate concentrations. So determined were V_{MTD}, $V_{SH(1)}$, and the ratio V_{MS}/V_{MTR}, the latter variable being chosen because the steady state of $MeFH_4$ depends only on this ratio rather than individual V_{max} values. (In final refinement of fits across all folate data, mean observed FFH_4 and $MeFH_4$ concentrations were replaced by their 10% larger upper standard deviation estimates.) To make Equations 7.3–7.5 solvable in terms of just the V_{MTD}, V_{SH}, and V_{MS}/V_{MTR} unknowns (and not also $V_{SH(2)}$, V_{FTS}, V_{TS}, V_{GAR}, and V_{AT} as follows from substitution of Equation 10 into Equations 7.3–7.5), we essentially zeroed $V_{SH(2)}$ and V_{FTS} by setting them equal to their L1210 estimates (Jackson and Harrap, 1973) (with these parameter values the SH(2) and FTS reactions were estimated to be minor contributions to the flux balances at CH_2FH_4 and FFH_4), set each of the purine reaction rates at FFH_4 (r_6 and r_7) equal to the upper bound experimental GAR synthesis rate (G_0), and determined V_{TS} by equating the experimental thymidylate synthesis rate (U_0) with r_9. The V_{MS}/V_{MTR} ratio determined from simultaneous solution of the three folate balance equations was finally used to scale the isolated enzyme V_{max} values for these two enzymes up and down by 1.87. Thus, were derived the V_{max} values (V_i) in Table III for SH, MTR, MS, MTD, TS, and FTS.

The steady state balance on FH_2 could not uniquely establish a value for the ternary rate constant of DHFR (k in Table III) because the concentration of FH_2 at steady state was too low to be detectable. However, it could be used to determine if the k value taken from isolated enzyme measurements on DHFR (Allegra *et al.*, 1985c) led to a predicted steady state concentration of FH_2 that was consistent with its experimental detection limit. This estimate of k (given in Table III) led to an FH_2 concentration of 3.6 nM, a figure lying well below the 50–100 nM detection limit of our assay and indicative that k does not exceed its maximum allowable experimental value.

To complete the steady state folate model, V_{max} values for the purine reaction enzymes remained to be specified, *i.e.* those for GT, AT(7), and FA. Two of these were derived by noting that, at steady state, each of the reaction fluxes involving these enzymes (r_6, r_7, and r_{13}) must equal the known GAR synthesis rate, G_0. In the case of AT(7), AICAR was set equal to its experimental value (Allegra *et al.*, 1987), K_m values were the model values in Table III, and equality of r_7 and G_0 led to the V_7 value in Table III. In the case of FA, the same

TABLE IV

Miscellaneous kinetic parameters

All parameters have been obtained from our MCF-7 cells except the formate concentration and the nonenzymatic rate constants. These values apply to both cycle-independent and cycle-dependent cells, except U_0. In the case of an asynchronous mix of G- and S-phase cells, the population averaged TS synthesis rate is as above but it arises from a 3.16-fold larger S phase-U_0 and a 0.158-fold smaller G phase-U_0.

Parameter	Variable	Value
Nonenzymatic HCHO reaction		
Production rate constant (h^{-1})	h_p	23.2[a]
Loss rate constant (μM^{-1} h^{-1})	h_l	0.3[a]
dUMP synthesis rate		
(Average drug-free cell) (μM h^{-1})	U_0	5.1 (5.2 expt)[b]
GAR synthesis rate		
(Drug-free cell) (μM h^{-1})	G_0	650.0 (415 expt.)[c]
DHFR concentration		
(Drug-free cell) (μM)	D_0	0.64[d]
DHFR synthesis rate ratio (k_0/k_{00})	α	3.31[d]
DHFR degradation rate (h^{-1})	k_d	0.03[d]
Influx transport constants for MTX1[e]		
Maximal rate (μM h^{-1})	V	82.2[d]
Michaelis constant (μM)	K_t	8.2[d]
Efflux transport constants		
MTX_1 (h^{-1})	L_1	4.65[d]
MTX_2 (h^{-1})	L_2	0.00[f]
MTX_n, $n = 3, 5$ (h^{-1})	L_n	0.063[d]
Polyglutamation rate constants (h^{-1})		
Glutamation	$L_{n,n+1}$ $n = 1,4$	0.129, 0.369, 0.118, 0.185[d]
Deglutamation	$L_{n+1,n}$ $n = 1,4$	0.195[7], 0.025, 0.031, 0.191[d]
Constant substrate concentrations (μM)		
Serine		123.3
Formate		500 (L1210)
ATP		2980
Glutamine		7170
Glycine		1600
$NADP^+$		6.73
NADPH		294
HCYSH		10

[a] Jackson, 1980.
[b] [^{3}H]Deoxyuridine incorporation into DNA.
[c] [^{14}C]Glycine incorporation into RNA.
[d] Morrison and Allegra, 1987.
[e] Together with L_1, these values account for a medium to intracellular MTX_1 ratio of 1.73.
[f] L_2 (efflux rate constant for MTX_2) is not algebraically separable from the hydrolysis component of L_{21}; hence L_2 has arbitarily been set equal to zero and L_{21} is a lumped deglutamation constant accounting for both efflux and hydrolysis of MTX2.

approach was employed. However, while the glutamine concentration was known for MCF-7, the control cell FGAR concentration and K_m values had to be estimated from the L1210 cell line (Jackson, 1980). Consequently, the FA reaction in our model primarily serves as a reaction flux bridge between FGAR and AICAR, a rigorous representation provided FGAR does not saturate the enzyme. On the other hand, FGAR concentrations computed from this reaction are not necessarily accurately scaled to the MCF-7 line and they should not be expected to agree with experiment. In the case of GT, the $G_0 = r_6$ relation could not be used to calculate V_{GT} for the intact cell because no experimental value for the steady state GAR concentration was available; hence V_{GT} was set equal to its isolated enzyme value (Allegra *et al.*, 1985c) and the G_0 balance was used to estimate GAR at steady state.

The steady state concentrations of GAR, FGAR, AICAR, and dUMP consistent with the parameters of Table III are 0.74 mM, 16 μM (see comment above), 3.4 μM, and 22 μM. Final steady state values for the folate concentrations were 3.6 nM (FH_2), 0.46 μM (FH_4), 0.26 μM (CH_2FH_4), 1.64 μM ($MeFH_4$), and 0.99 μM (FFH_4). No MCF-7 experimental data exists against which to compare the GAR and FGAR concentrations but AICAR has been forced equal to its MCF-7 value and the (population-averaged) dUMP value of 22 μM compares with 20 μM found for L1210 by Jackson (1980).

The principal finding from the steady state folate fittings was that experimental data from asynchronous populations were reproduced by cycle-independent model V_{max} values that never differed from isolated enzyme V_{max} values by more than 2-fold. Furthermore, this occurred with thymidylate and purine synthesis rates confined to their experimental range.

Methotrexate-dependent Folate Model (Cell Cycle Independent)—The folate cycle model was next used to predict the behavior of folate pools in MCF-7 cells exposed in culture to 1 μM MTX (Allegra *et al.*, 1986). This required that MTX inhibition, both direct and indirect, be described by appropriate inhibition constants.

Initially the numerical values of these constants were taken as their experimental values in Table III. In addition, the production of FFH_2 behind the MTX-induced DHFR block requires that the reactions (r_{11} and r_{12}) responsible for gain and loss of this species be parameterized. Accordingly, the binding constants for FFH_2 and FFH_4 in reaction 12 were taken identical to those in reaction 7, except for reversed roles as substrate and inhibitor; AICAR, FH_2, and MTXn played the same roles and had the same numerical values in both reactions. Following Baram *et al.* (1987), the V_{max} for AT with FFH_2 as substrate was taken to be comparable (initially

identical) to that with FFH_4 as substrate, and the FDS first order rate constant was then chosen to force the model to reproduce the observed FFH_2 concentration after 21 h of exposure to 1 μM drug.

These initial inhibition parameters revealed that much of the experimental folate pool behavior was reproduced by the model. Over 21 h of exposure, FH_2, FFH_2, and FH_4 pools closely followed experimental time courses, while the $MeFH_4$ pool declined a little too rapidly (falling to about 50% of the experimental value by 10–15 h of exposure), and both the CH_2FH_4 and FFH_4 pools tended to level out at values that were also about 50% of the experimental values. Most significantly, these latter two pools did not collapse essentially to zero as predicted in earlier models where nearly all folates were being trapped in the FH_2 pool.

Improved fits were then sought by varying inhibition constants within reasonable estimates of their experimental uncertainty. We first performed a sensitivity analysis in which each inhibition constant in the model was altered by a fixed percentage while holding all others constant, and corresponding changes in pool sizes at various times of exposure were computed. This procedure revealed that the inhibition constant most strongly affecting the time course of $MeFH_4$, while leaving other pools relatively unaffected, was that of FH_2 at MTR. Similarly, the roughly steady levels of CH_2FH_4 and FFH_4 achieved by 21 h of drug exposure were, respectively, most effectively controlled by the inhibition constants of MTX2 to MTX4 at TS and the inhibition constants of FH_2 and FFH_2 at GT. It was further discovered that best fits to the experimental data were found near the allowable extremes of these inhibition constants. Because different investigators, experimenting at different times, have only been able to reproduce the MCF-7 inhibition constants within factors of two (in contrast to the precision variance in a given experiment which is much smaller), the lower extreme values of 1 and 5 μM were chosen for FFH_2 and FH_2 inhibition at GT, and values of 0.08, 0.07, and 0.065 for MTX2 to MTX4 inhibitions at TS (Table III). In the case of the FH_2 inhibition constant at MTR, no MCF-7 value was available. However, it was found that the best fit to the $MeFH_4$ profile was obtained with an inhibition constant 10-fold that measured for purified pig liver enzyme (Matthews and Baugh, 1980). (Fits to other folate profiles are negligibly affected by this change.) This 10-fold increase apparently lies outside the range of the pig liver enzyme measurements, but since we are dealing with another species, we let the higher estimate stand (also see Fig. 6). Finally, we found that AICAR concentrations predicted by our model were slightly improved (with no effect on folate pool fits) by lowering the V_{max} for FFH_2 at AT to its lowest extreme value (approximately equivalent to the lower 96% confidence limit of V_{max}/K_{FFH2}) (Baram *et al.*, 1987).

Fits to the experimental folate data using the cycle-independent model parameters of Table III are shown in Figs. 2–6. Concentrations of each folate are shown as a function of time and compared to the experimental data of Allegra *et al.*, 1986. Experimental data are shown as measured except for increases in all folate concentrations at 21 h to account for an observed 24% loss in total folate by this time. With this correction, both experiment and model conserve folate, leading to a common basis for comparison between the two.

Fig. 2 shows that the time course of FH_2 is well-represented by the model. FH_2 rises to nearly 90% of its drug induced maximum in 2 h of exposure, and then remains relatively level over the next several hours. Fig. 3 exhibits the time course of FFH_2 and reveals that our model overpredicts FFH_2 concentrations, including early times. These concentrations

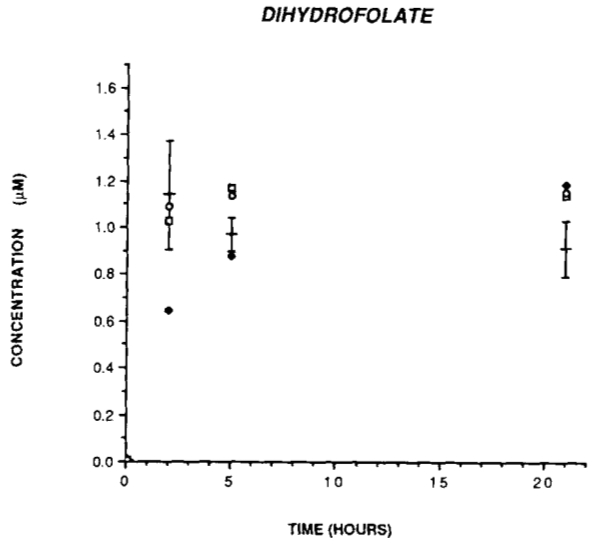

FIG. 2. **Concentration profile of dihydrofolate polyglutamate following exposure to 1 μM MTX.** *Bar* denotes experimental values ± 1 S.D.; *open square* is average folate concentration from the cell cycle-independent model; *diamond* is average folate concentration from the cycle-dependent model; *circle* is the folate concentration in a cell continually in S-phase. At zero time, only *open square* and *circle* are plotted; while these appear identical on this scale, the *circle* (S-phase) value is about 3-fold larger.

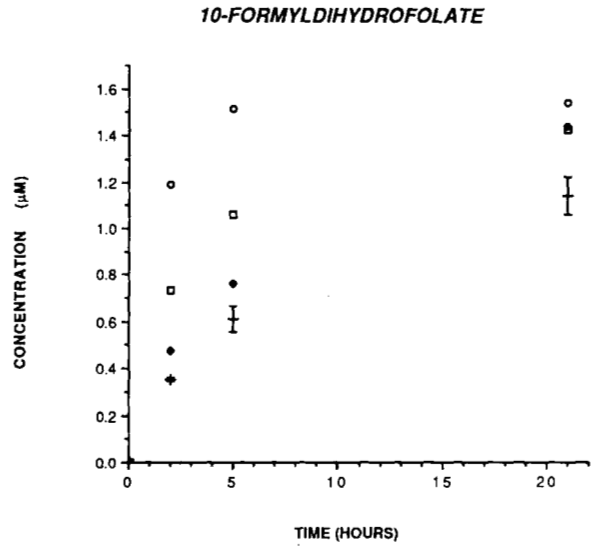

FIG. 3. **Concentration profile of formyldihydrofolate polyglutamate following exposure to 1 μM MTX.** Symbols are the same as in Fig. 2.

can be lowered by reducing the value of the reaction constant, k_{FDS}, but only at the cost of elevating the FH_2 substrate concentration. Fig. 4 shows the concentration profile for CH_2FH_4. The model values decline rapidly, due to initial build-up of folates in the FH_2 pool, and then level out at values only slightly lower than experiment (Allegra *et al.*, 1987) and generally within two standard deviations of the experimental data. To a great extent, this leveling of the model's CH_2FH_4 concentration occurs because of inhibition of TS by MTX di- and triglutamates. The FFH_4 concentration profile is shown in Fig. 5 to be well reproduced by the model. Very close agreement exists between model and experiment at early times, giving way to a small underprediction by the model by 21 h of exposure. Indirect inhibition of GT, by FFH_2 and FH_2 and of AT by FH_2 play a more important role in

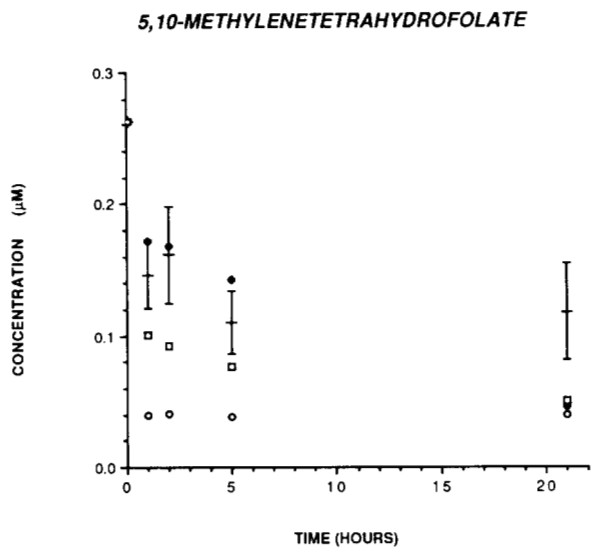

FIG. 4. **Concentration profile of 5,10-methylenetetrahydrofolate polyglutamate following exposure to 1 μM MTX.** Symbols are the same as in Fig. 2. Note change of concentration scale in this figure. At zero time, only *open square* and *circle* values are plotted; these values are essentially identical because their associated parameter differences occur in the TS pathway whose normal flux is small and of little impact on the tetrahydrofolate pools.

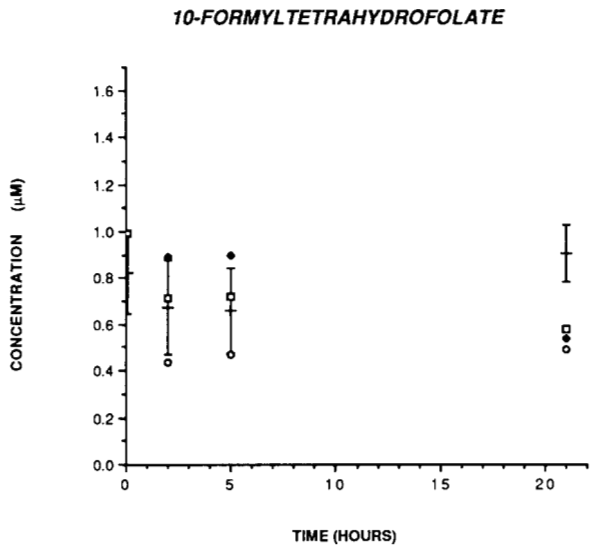

FIG. 5. **Concentration profile of 10-formyltetrahydrofolate polyglutamate following exposure to 1 μM MTX.** Symbols are the same as in Fig. 2, and zero time values are as described in Fig. 4.

trapping folates in this FFH_4 pool at early times than do direct MTX inhibitions. This is because the MTX*n* inhibition constants are relatively large and MTX*n* concentrations have not yet climbed to significant levels by the 2-h point when FFH_4 is clearly being retained in this pool (see MTX*n* plots in Fig. 2 of Morrison and Allegra, 1987). Fig. 6 compares experimental results for $MeFH_4$ with two model predictions. This folate pool is most sensitive to our choice of inhibition constant of FH_2 at MTR ($K_3^{FH_2}$). A low value for this constant increases inhibition of the enzyme and restricts the ability of MTR to resupply some of the $MeFH_4$ lost as this "storage" pool decays away, much ultimately to FH_2 and FFH_2. The lower cycle-independent model results in Fig. 6 correspond to the $K_3^{FH_2}$ value of 0.4 μM in Table III (10-fold the pig liver value) while the upper model results correspond to a $K_3^{FH_2}$

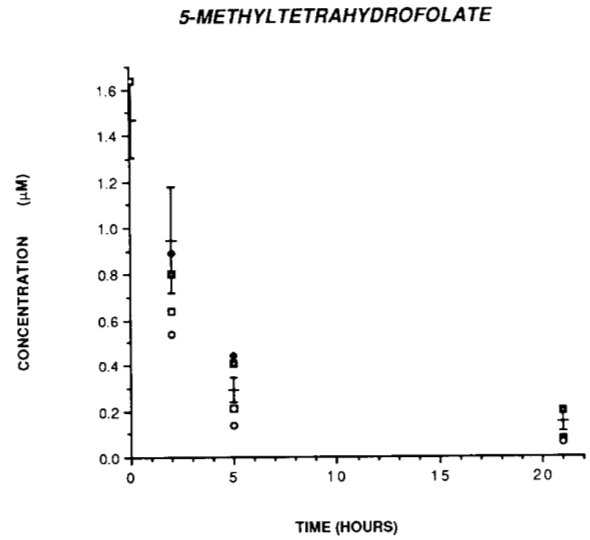

FIG. 6. **Concentration profile of 5-methyltetrahydrofolate polyglutamate following exposure to 1 μM MTX.** Symbols include those of Fig. 2, where all results are derived from models using an FFH_2 inhibition constant at MTR of 0.4 μM. In addition, the *closed squares* give another cell cycle-independent result with a decade larger value of this inhibition constant, *i.e.* 4.0 μM. Zero time values are as described in Fig. 4.

value that is still larger at 4 μM. These two results demonstrate the sensitivity of the $MeFH_4$ fit to $K^{FH_2}{}_3$ and indicate that the best fit data is obtained at values that are at least 10-fold above the 0.04 pig liver value. The last folate for which we computed a concentration profile was FH_4. This species began with 14.8% of the total folate pool at time 0, declined rapidly to 4.7% within 1 h, and then gradually fell to 2% by 21 h of exposure. Experimentally, this species is not observable after just 2 h of exposure. This agrees with our model, however, because the precipitious decline over the first hour drops an already small initial folate concentration below the limit of detectability.

Other cycle-independent model results may be compared with experimental data. In particular, rates of thymidylate and purine synthesis in the presence of drug may be calculated from the thymidylate reaction r_9 (Equation 10 and Table II) and the net AICAR formylation rate (Equation 7.11), respectively. Model thymidylate synthesis rates, expressed as a percentage of the cycle-averaged control (drug-free) rate U_0, are given in Table V for three MTX dosage concentrations at three times of exposure. Also given are corresponding experimental estimates of the population averaged MCF-7 thymidylate synthesis rates as determined by the incorporation of [^{3}H]deoxyuridine into DNA (Allegra *et al.*, 1986). However, these experimental rates were derived without correction for the increasing dilution of ^{3}H-dUMP by nonlabeled dUMP that accumulates behind the TS block. Since it is known from other studies that this pool may rapidly expand by a factor of two to eight when TS is completely blocked (Jackson and Harrap, 1973; Myers *et al.*, 1975), it is reasonable to assume that the true experimental values corresponding to Table V are elevated by similar factors, especially at the two higher MTX doses where TS inhibition is more complete. Hence with this factor considered, the model estimates of synthesis rates appear to be in reasonable agreement with experiment. The largest difference between model and experiment occurs at the 12-h point for 0.1 μM MTX. We investigated whether this result might have resulted from an underestimation by the cycle-independent model of the amount of free higher MTX polyglutamate inhibitor available for TS inhibition at

TABLE V

Thymidylate synthase activity after methotrexate exposure

Conc.		Time (h)		
		1	2	12
μM		*% Control*		
10	Model	2.9	1.6	0.3
	Experimental[a]	0.7	0.1	ND[b]
1	Model	10.9/6.8[c]	5.9/4.8[c]	0.8/3.5[c]
	Experimental	1.4	0.2	ND
0.1	Model	19.1	15.1	13.3
	Experimental	29.8	14.1	ND

[a] Relative TS activity as determined by [^{3}H]UdR incorporation into DNA. Activity is uncorrected for dilution by the expanding dUMP pool behind the drug block, and thus experimental values overestimate the true inhibition by MTX.

[b] ND, not detectable.

[c] First entry from cycle-independent model, second from cycle-dependent model.

this low dose. However, raising the polyglutamation rate within reasonable uncertainty and totally eliminating DHFR induction failed to depress the model's percentage below 4%.

Fig. 6 compares cycle-independent model estimates of purine synthesis rates with experimental values obtained by the incorporation of [^{14}C]glycine (Allegra *et al.*, 1986) into adenine and guanine. Here the 1 μM MTX model predictions reproduce a rapid decline of purine synthesis within 1–2 h of exposure followed by a leveling off of activity considerably above zero for the next 20 h. Model results are somewhat higher than experiment, reaching 25% of control by 21 h while experiment has declined to 15%. The later 12- and 21-h predictions, respectively, lie just above and at the upper first standard deviation limit of each experimental point. One may not increase the experimental value by a factor analogous to the dUMP pool expansion correction at TS because the corresponding purine substrate pool, glycine, exchanges relatively rapidly across the cell membrane and thus maintains a constant intracellular pool size.

These purine synthesis rate percentages are very insensitive to changes in inhibition constant values at GT and AT; GT inhibition tends to control the rate, and decreased K_i values at GT are compensated by an increased FFH_4 concentration. Lowering the substrate activity of FFH_2 at AT by two-thirds, while keeping FFH_2 and FH_2 at 21 h matched to experiment by lowering k_{FDS}, also has very little effect on folate pools or the purine synthesis rate, principally because little change will occur at GT if FFH_2 is held fixed at its experimental value.

Effects of Cell Cycle-dependent Enzymes—Now considered are the effects of introducing cell cycle dependence into the folate model, primarily through the phase-dependent activities of TS and DHFR. To accomplish this, the experimental asynchronous populations, whose drug-response behavior is the modeling focus, are considered to consist of G- and S-phase cells where G-phase cells have only a small percentage of the activities of their S-phase counterparts. In a drug-free cell population (control), these cells are exponentially distributed over the cell cycle with twice the number of cells at beginning G_1 as present at the end of G_2 (see "Appendix"). However, when this population is exposed to 1 μM MTX, cells initially in S-phase are trapped there (because normally high thymidylate flux renders them vulnerable to a TS block) while those in G-phase continue to move through G_2/G_1 at nearly normal speed (estimated purine synthesis is ~80% of normal) until they too become trapped in S-phase.

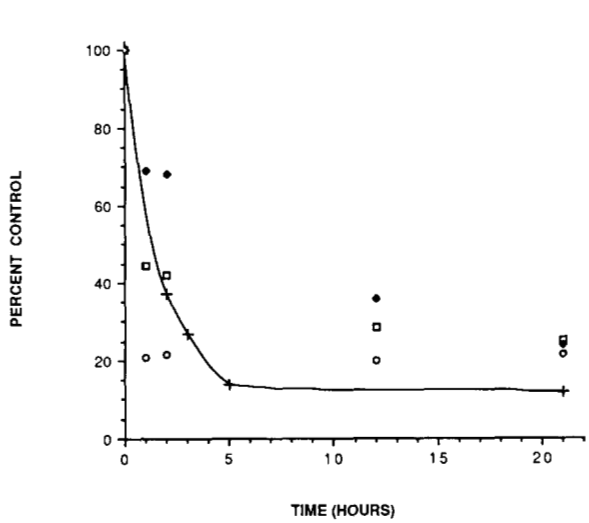

FIG. 7. **Purine synthesis rates, relative to control, following exposure to 1 μM MTX.** *Crosses* denote experimental points; all other symbols are the same as in Fig. 2. Experimental purine synthesis rates were determined by labeled glycine incorporation into the purine bases as described by Allegra *et al.*, 1986.

These concepts, together with known MCF-7 cell cycle parameters[2] and with the maturity-time model of the cell cycle (Rubinow, 1968; Aroesty *et al.*, 1973), allow the number of cells in both G- and S-phases to be estimated for any time after the beginning of drug exposure (see "Appendix"). In turn, these may be used to compute population-averaged folate concentrations, as well as thymidylate and purine synthesis rates, for comparison to experimental data.

In order to establish the likely magnitude of cycle-dependent enzyme effects, we have somewhat arbitrarily chosen TS and DHFR activities in G to be 5% of their S-phase values. This percentage reflects the 6–12-fold S/G_1 TS activity ratio reported for L1210 *whole cells* (Rode *et al.*, 1980) increased by a small factor to account for desynchronization effects of the assay. Presumably, this increased activity does not arise from increased TS mRNA synthesis, as observed in 20-fold TS activity increases in cells undergoing quiescent (G_0) to proliferating state transitions (Navalgund *et al.*, 1980; Jenh *et al.*, 1985; Ayusawa *et al.*, 1986; Ali Imam *et al.*, 1987), but rather from some form of post-translational control that operates across cycle phases in the proliferating state alone. While stability of the TS enzyme (half-life of 20 h) leads one to expect small TS cycle-dependence, as in fact observed in *cell extracts* from several cell lines, the report of Rode *et al.* (1980) indicates that other factors are operative in the intact cell. For MCF-7 cells, the 5% activity ratio is only taken as a likely lower limit. We also apply this ratio to DHFR, although it is generally less cycle dependent than TS (Navalgund *et al.*, 1980), in the anticipation that exaggerated enzyme cycle-dependence will tend to bound the estimates of its effects.

The results of carrying over this assumed G/S ratio to our MCF-7 model, and the comparison with experimental values, are shown in Figs. 2–7 and Table V. The parameters of this folate model are identical to the cycle-independent values in Tables III and IV, except for the entries representing the activities of TS (V_9) and DHFR (k ternary) and the drug-free synthesis rate (U_0), each of which are increased 3.16-fold and decreased 0.05 × (3.16)-fold for pure S- and G-phase cells, respectively. The 3.16 factor arises from the proportion of

[2] N. Brunner, personal communication.

control cells in S-phase and accounts for the predominance of TS and DHFR activity in S-phase cells; the 0.05 factor formalizes the assumption that G-phase activities are only about 5% of those in S-phase. Other V_{max} values, especially those derived from the earlier forced fitting of the control cell folate concentrations, are unchanged because the TS-associated folate flux is small in this case and even large cycle-dependent changes in TS/DHFR activities have little effect on other folate balances.

Figs. 2–6 exhibit two sets of cycle-dependent results. One consists of the population-averaged concentration profiles that are directly comparable to the experimental results. It is apparent that the averaged concentration fits are very similar to the results from the cycle-independent model. $MeFH_4$ results are quite similar. Cycle-dependent FH_2 is smaller after 2 h of drug exposure but very similar thereafter, and FFH_2 better agrees with experimental data. Both the CH_2FH_4 and FFH_4 profiles again exhibit relatively large concentrations over 21 h of exposure, although the profiles exhibit an inflective decline in the vicinity of 10 h due to the loss of the last G cells as they move into S-phase. The second set of results shown in the figures are the folate concentrations characteristic of those cells which began and remained in S-phase throughout the drug exposure. Here a different pattern emerges in which more folate is converted to FFH_2 via FH_2 at early exposure times (Fig. 3), resulting in reduced CH_2FH_4 and FFH_4 pools (Figs. 4 and 5) relative to the cycle-independent estimates. They do not approach zero, however, remaining at about 15 and 50% of the control over the full exposure period because inhibitions by FH_2 and FFH_2 at GT as well as MTX2/3 at TS are still sufficiently strong to limit folate depletion. (If all FH_2 and FFH_2 inhibitions are suppressed, then the S-phase CH_2FH_4 pool falls by another factor of 3.5 and the FFH_4 pool by 7.5.) Had experimental mean values been used for all the inhibition constants at TS and GT, the S-phase CH_2FH_4 pool would have shown greater depletion, leveling off near 9% of control.

Finally, we note that folate pool behavior at long times (*e.g.* 21 h) is largely determined by S-phase parameters, since this time is sufficient for all but a negligible portion of cells to enter S-phase and respond accordingly. In addition, even if G-phase activities are lower than we have assumed, S-phase activities will remain practically unchanged from those above because any further change would no longer allow thymidylate synthesis in the S cells of the asynchronous control population to properly account for the experimental population average. Hence, a pool such as CH_2FH_4 should still respond at long term much like that exhibited in Fig. 4.

Average purine and thymidylate synthesis rates computed from the cycle-dependent model are presented in Fig. 7 and Table V. The purine results asymptote to the same experimental value at 21 h but considerably overestimate synthesis rates in the 2–10 h range relative to the cycle-independent model. Averaged thymidylate synthesis results following 1 μM MTX exposure are shown in Table V, and generally present the same pattern as observed before.

DISCUSSION

The models that we have constructed account for folate cycle behavior in intact MCF-7 human breast cancer cells exposed to MTX in the vicinity of 1 μM concentration. Population-averaged folate pools are well described, both by cycle-independent and cycle-dependent models (the latter with G-phase TS/DHFR activities down at least to 5% of S-phase). Purine synthesis rates are overpredicted in the near term by both models but more so by the cycle-dependent model. Thymidylate synthesis rates are qualitatively reproduced, but complete comparison with experiment requires additional data on the dynamics of the dUMP pools in MCF-7 cells following drug exposure. Consistent with these results are the findings that all normal substrate-binding constants (bisubstrate Michaelis constants) are equal to their isolated enzyme experimental values, while V_{max} values operative in intact cells never differ from our isolated enzyme values by more than a factor of two. Furthermore, model constants describing the inhibition of MTR, GT, AT, TS, and DHFR by MTX*n*, FH_2, and FFH_2 are either identical to or within 2-fold of their experimental values except for an order-of-magnitude increase in the pig liver K_i of FH_2 at MTR.

Of importance is the observation that, in the presence of MTX, the known pattern of reactions and parameter values reproduces the relatively constant concentration profile of FFH_4 and the non-zero profile of CH_2FH_4 seen experimentally after its initial drop. Prediction of this cell-averaged pool behavior has emerged from both the cycle-independent and cycle-dependent formalisms. Furthermore, the cycle-dependent formalism has also allowed us to estimate FFH_4 and CH_2FH_4 profiles in pure S-phase cells, where we again found that FFH_4 and CH_2FH_4 pools were maintained at levels significantly above zero. Depletion of folate, particularly at CH_2FH_4, played a greater role in these S cells than is apparent in population-averaged experimental data (in agreement with suggestions of Seither and Goldman, 1988) but pool sizes were still maintained at 15% (CH_2FH_4) and 50% (FFH_4) of control values after 21 h of drug exposure.

Our kinetics indicate that much FH_4, $MeFH_4$, and some FFH_4 is rapidly diverted into FH_2 (and thence to FFH_2) following first exposure to drug. Together these (highly polyglutamated) forms then quickly begin to inhibit GT and AT, thus trapping FFH_4 behind the block at levels comparable to its initial fraction of total folate. At these early times (<1 h) as well as for several hours thereafter, MTX polyglutamates play a negligible role at these enzymes because their concentrations are too small to be a significant fraction of their K_i values. CH_2FH_4 also undergoes a rapid initial drop as the dihydrofolate pools are built-up. However, it subsequently achieves a relatively stable level as MTX2 and MTX3 begin to inhibit TS and the FFH_4 pool provides a reduced folate presence. FH_2 and FFH_2 continue to play a role in determining TS activity but they tend to modulate the MTX polyglutamate effects. Our earlier MTX polyglutamate model (Fig. 2 of Morrison and Allegra, 1987) showed that MTX2 rose quickly and neared a plateau value within 3 h, with MTX3 following rapidly behind. Thus, both concentrations may rise well above their inhibition constants at TS by 3 h, causing conversion of CH_2FH_4 into FH_2 and FFH_2 to be blocked. While these interactions may have been qualitatively suggested by the relative order of magnitude of isolated inhibition constants and related pool sizes, our model gives their existence added weight since it has demonstrated that quantitative self-consistency exists between the underlying isolated enzyme values and folate mass dynamics over the entire 21-h period of experimental observation.

The choice of reaction mechanism by thymidylate synthase is an important factor in obtaining a model that maintains the CH_2FH_4 pool near its experimental value. The TS model we have used is a three-site model, one for dUMP, one for CH_2FH_4 and FFH_2, and another for MTX*n* and FH_2, based upon the patterns of non-, un-, and competitive inhibition observed by Allegra *et al.* (1985) when TS is inhibited, separately, by each potential inhibitor. This model allows both FFH_2 and any of the MTX*n* or FH_2 to bind simultaneously

to TS, provided one assumes that FFH_2 is physically sited very similarly to CH_2FH_4 so that inhibition patterns observed with normal substrate also apply to FFH_2. If this were not true and, as a hypothetical example, FFH_2 could not bind to enzyme simultaneously with MTX*n* or FH_2, inhibition of TS would be substantially reduced, leading to a halving of the computed 21-h CH_2FH_4 pool size shown in Fig. 4. This amount of CH_2FH_4 pool reduction is very nearly the equivalent of doubling the MTX2 to MTX4 inhibition constants at TS.

Another aspect of the TS reaction mechanism is that the final results are quite insensitive to the choice between a sequential mechanism with dUMP binding first to enzyme or a random order mechanism. This occurs because the binding constant of dUMP to TS (1.8 μM) is considerably less than the pool size of the dUMP (22 μM) required for TS synthesis at steady state to match experiment. Thus, in either mechanism, most enzyme is bound to dUMP, and little difference exists between the two (~1% changes in pool sizes).

The few inhibition constants in Table III that have been shifted from their experimental means constitute a set that strongly determines the balance point between model and experimental descriptions of the purine synthesis rate and CH_2FH_4 and FFH_4 pool sizes. Sensitivity of these rates and pool sizes to parameter variation can be demonstrated by example from the cycle-independent model. If the experimental mean values for the inhibition constants of MTX2–4 were employed instead of the halved values in Table III, more folate would flow to FH_2 causing a reduced folate flux via MTD to FFH_4, and the purine synthesis rate would be perfectly reproduced. Thymidylate synthesis rates would increase only slightly, from 11 to 12.5% of control at 1-h exposure and from 6.0 to 7.3% at 2 h, while still falling to 0.8% of control by 12 h. However (while constraining FFH_2 to mimic experiment by altering k_{FDS} and keeping all other parameters at their cycle-independent Table III values), this agreement would come at the expense of a 20–40% drop in the CH_2FH_4 profile, a 25–30% drop in the FFH_4 profile, and a 20–27% rise in the FH_2 profile over the 21-h MTX exposure period. If we considered 2-fold changes in the K_i values for FH_2 and FFH_2 at TS, then unlike the MTX K_i values, we would find little effect on the model's description of rates and pool sizes, as expected from a relative comparison of inhibitor concentration to K_i ratios. Likewise, rates and pool sizes are only moderately affected by 2-fold changes in the FH_2 and FFH_2 K_i values at GT; the decrease from the experimental values in Table III to the model values altered both the FFH_4 pool size and purine synthesis rates somewhat (the FFH_4 pool size rose by 15%, essentially to the experimental values), but at a small loss of fit to CH_2FH_4 whose profile declined an additional 6% below experiment.

While the purine flux is approximated by our model, purine intermediate concentrations and factors responsible for their magnitude are less well characterized. No MCF-7 experimental data exists against which to compare model GAR and FGAR concentrations. However, comparisons can be made in the case of AICAR. When its general level was set at the experimental drug-free steady state level, the corresponding V_{max} at AT (V_7), computed to force the flux through this enzyme to equal the experimental purine flux, agreed closely with the experimental V_{max} from isolated enzyme. Hence, under drug-free conditions, substantial self-consistency exists between overall purine flux, the isolated V_{max} at AT and AICAR concentration.

In the presence of 1 μM MTX, our model (both cycle-dependent and independent) predicts that population-averaged AICAR drops slowly to a near-plateau level of 50% of its drug-free value by 12 h of exposure. That it stays in the near-vicinity of its drug-free value agrees with earlier findings (Allegra *et al.*, 1986) that direct inhibition by MTX*n* and FH_2 keep the pool from dropping precipitiously, as might occur if only folate depletion depressed purine synthesis. However, our models are at variance with experiment in finding that AICAR levels decrease rather than increase. (Our particular cycle-dependent model indicates that AICAR levels increase in G cells and decrease in S cells, but the averaged cell value declines.) Two possible explanations for this have been investigated. One explanation is that FFH_2 is a poorer substrate at AT than represented by our V_{max} for this reaction (V_{12}) and hence acts more like a pure inhibitor, causing AICAR to back up to higher levels behind blocked AT. This explanation is probably incorrect. To cause AICAR levels to increase at all, we found that V_{12} would have to be decreased to a mere 0.1% of the activity found with FFH_4 as substrate, and this magnitude of decrease far exceeds the experimental uncertainty of the relative V_{max} obtained from isolated enzyme measurements. The second explanation is that FH_2 and/or MTX*n* might be better inhibitors at AT than represented by the inhibition constants of Table III. This appears more plausible. For instance, if the inhibition constant for FH_2 ($K_7^{FH_2}$) *were 5-fold lower at 0.6* μM, than AICAR rapidly increases above its drug-free value by 50% and remains above this value for the next 6 h before declining to a plateau level back near the drug-free value. On the other hand, a 5-fold change in K_i from its mean experimental value is large, and it is possible that other undiscovered explanations may be operative.

As developed, the folate model depends upon a large number of explicit variables and thus a large number of parameters. However, the specific responses of folate pools and purine and pyrimidine *de novo* synthesis rates modeled in this report do not uniquely depend on all the variables and constants listed in Tables III and IV, but rather on a critical combined subset of these. For example, in the reactions in which one substrate remains constant in the presence of drug (reactions at SH(1), MTR, MS, MTD, and FA), the corresponding Michaelis term which appears in the reaction rate denominator may be combined with the reaction V_{max} to form a single parameter ultimately taking its value from a fit to steady state folate pools and the purine reaction rate. The consequence of this is that if we had initially chosen other K_{2m} values, our V_{max} determinations would have compensated for the new choice of K_{2m} and the model folate dynamics would have remained invariant. Additional significance arises from this effective disappearance of Michaelis constants since they constitute a majority of the parameter values not available for the MCF-7 line. Thus our model is actually more MCF-7 specific than is evident with retention of these K_m values in the model. Likewise, the folate concentrations at several enzymes (MTR, MS, FTS, and more approximately, GT and AT) always lie sufficiently far below their Michaelis constant values (at dose levels considered by us) so that reaction rates at these sites are actually dependent on V_{max}/K ratios rather than full Michaelis expressions. Finally, we note that most of the MTX*n* binding to DHFR (again over the dosages and exposure periods considered by us) depends not as much on the full set of six association/dissociation rate constants as on the five equilibrium ratios. Thus, some parameter reduction could be applied to our model. However, we opt for the moment to leave the model in its more extensive form so that it more explicitly represents oft-considered phenomena associated with folate chemistry and remains in a form more easily adapted in the future for describing folate cycle perturbations.

CONCLUSIONS

Several overall conclusions may be drawn from the present modeling effort. First, the existing body of MCF-7 MTX-induced folate pool size responses, isolated enzyme kinetic constants, and purine/pyrimidine synthesis rates appear to form a quantitatively self-consistent data set. While agreement with experiment is not perfect, neither qualitative nor large quantitative differences were found, suggesting that the principal features that affect the type of experimental data examined have been identified. Stronger confirmation awaits measurement of the response of dUMP and purine intermediates to MTX and demonstration of more extensive comparisons with our thymidylate and purine dynamics. Meanwhile, the model provides a very good description of the human breast cancer cell in the presence of MTX for periods of up to 24 h and at dose levels ≤10 μM. Second, a cycle-dependence of TS and DHFR enzymes down to a G- to S-phase activity ratio of (at least) 5% has been calculated to have only a slight effect on population-averaged folate pools, but to depress CH_2FH_4 pools in S-phase cells to a stable level that nears 10% of control. Third, the kinetic importance of the FH_2 and FFH_2 species as inhibitors has been underscored by the need to include their inhibition kinetics in order to quantitatively account for the stable population-averaged CH_2FH_4 and FFH_4 pools seen after drug exposure. Exclusion of these inhibitions from either the cycle-independent or dependent models led to substantial reduction of both pools, and in the case of cycle dependence, to significant depletion. Finally, the existence of a quantitatively self-consistent model means that it may now serve as an improved vehicle for investigation of other human cell folate reactions. It should be particularly well suited for investigation of the folate dynamics of therapeutic agents such as citrovorum factor.

Acknowledgment—We gratefully acknowledge the careful and dedicated assistance provided by Shelley R. Hankins during the computational aspects of this research.

APPENDIX

This appendix outlines the method used to calculate population averages of the folate pools, purine, and thymidylate synthesis rates. The essence of the approach is to obtain, from a cell cycle model, at any time t following the initiation of MTX exposure, the residence time distributions for cells in S-phase and the combined G_1/G_2 phases of the cell cycle. For this same time t, values of the folate variables for a given cell are computed from the above folate model in two steps, the first corresponding to integration over the time t' when the cell is resident in G_1/G_2 (with lower TS and DHFR activities) and the second to integration over the remaining time $t - t'$ when the cell is resident in S-phase (with higher activities). The residence time distributions are then used to average over all such folate variables to yield population-averaged pool and nucleotide synthesis rates.

We describe the cell cycle using the maturity-time model of Rubinow (1968) but, for convenience, alter the usual order of phases (G_1, S, G_2) to G_2, G_1, S. We consider the cell population to be characterized by a single cycle time T with components $T_{G1} = 12$ hr, $T_S = 6$ h, and $T_{G2/M} = 2$ h.[2] Position in the cycle is then denoted by a variable μ ranging from 0 to 1 with intermediate values μ_1 and μ_2 respectively denoting the locations of the G_2/G_1 and G_1/S boundaries (0.1 and 0.7, respectively). A control MCF-7 population is exponentially distributed across μ, subject to the requirements that equality of cell number exists at $\mu = 0$ and 1 and that a cell-doubling discontinuity exists at μ_1. Denoting the number density of cells at cycle position μ at any time by $n(\mu,t)$, then control cells or drug-treated cells at zero time have

$$n(\mu, 0) = N_0(2 \ln 2)2^{-\mu+\mu_1-\delta} \quad \text{(A1)}$$

where $\delta = 1$ in the G_2 region ($0 < \mu \leq \mu_1$), $\delta = 0$ in the G_1 and S regions ($\mu_1 < \mu$), and N_0 is the initial number of cells.

In drug-treated populations, the G_2/G_1 portion of this distribution may be thought of as moving to the right toward the G_1/S boundary with the proviso that each cohort that crosses the G_2/G_1 boundary double its number as it undergoes mitosis. (Because G-phase movement remains ~80% of normal in the presence of 1 μM drug, for simplicity, we neglect any drug-induced extension of the G transit time in subsequent treatment.) Cells originally in S-phase remain there because of negligible exit from this phase at 1 μM MTX. This allows us to construct distributions at any time by shifting the initial distribution given in Equation A1. This is done for four time frames, (I) $0 < t \leq \mu_1 T$ during which all initial G_2 cells will double and move into G_1 phase (but will not reach S due to the longer length of G_1 in the MCF-7 line), (II) $\mu_1 T < t \leq (\mu_2 - \mu_1)T$ by the end of which all initial G_1 cells will have entered S phase, (III) $(\mu_2 - \mu_1)T < t \leq \mu_2 T$ during which the original G_2 cells enter S-phase, and (IV) $t > \mu_2 T$ when all cells are in S-phase.

The number of cells in both G_1 and G_2 at time t is thus

$$N_G(t) = \int_0^{\mu_1 - t/T} n(\mu, 0)d\mu + \int_{\mu_1 - t/T}^{\mu_1} 2n(\mu, 0)d\mu + \int_{\mu_1}^{\mu_2 - t/T} n(\mu, 0)d\mu \quad \text{(I, II)} \quad \text{(A2.1)}$$

for t in time frames I and II. (If $\mu_1 - t/T$ becomes negative, it is replaced by zero.) The first integral accounts for $G_2 \rightarrow G_2$ movement, the second for $G_2 \rightarrow G_1$ as well as mitotic doubling, and the third for $G_1 \rightarrow G_1$ movement. The integration limits are set by observing that the passage of time t corresponds to a shift of the initial distribution in μ by t/T. Hence, the first integral states that only that portion of the initial distribution lying between $\mu = 0$ and $\mu_1 - t/T$ will remain in G_1 at t. For time frames III and IV,

$$N_G(t) = \int_0^{\mu_2 - t/T} 2n(\mu, 0)d\mu \quad \text{(III)} \quad \text{(A2.2)}$$

$$= 0 \quad \text{(IV)} \quad \text{(A2.3)}$$

Equation A2.2 only accounts for initial $G_2 \rightarrow G_1$ transitions and associated cell doubling, while Equation A2.3 reflects the entry of all original G-phase cells into S. Carrying out the integrations of Equations A2 using Equation A1 leads to

$$N_G(t) = N_0\left[\left(1 - 2^{1+\mu_1-\mu_2}\right)2^{t/T} + 2^{\mu_1}\right] \quad \text{(I)} \quad \text{(A3.1)}$$

$$= 2N_0\left[2^{\mu_1} - 2^{\mu_1-\mu_2+t/T}\right] \quad \text{(II,III)} \quad \text{(A3.2)}$$

$$= 0 \quad \text{(IV)} \quad \text{(A3.3)}$$

Note that for G-phase cells, $N_G(t)$ is also the residence time distribution since any cell still in G_1 or G_2 at time t has never been anywhere else.

The number density of cells in S-phase at time t having had a prior residence time t' in G-phase and residence in S of $t - t'$, $n_S(t - t', t)$ is

$$n_S(t - t') = n(\mu_2 - t'/T, 0) \; 0 < t' \leq t \quad \text{(I,II)} \quad \text{(A4.1)}$$

$$n_S(t - t') = \beta n(\mu_2 - t'/T, 0) \quad \text{(III, IV)} \quad \text{(A4.2)}$$

where $\beta = 1$ if $0 < t' \leq (\mu_2 - \mu_1)T$ in domains III and IV, and $\beta = 2$ if $(\mu_2 - \mu_1)\, T \leq t' < t$ in domain III or if $(\mu_2 - \mu_1)\, T <$

$t' \leq \mu_2 T$ in domain IV. In addition, the number of cells originally in S, N_S, can be obtained by appropriate integration of Equation A1 as

$$N_S = N_0 \left(2^{1+\mu_1-\mu_2} - 2^{\mu_1} \right) \tag{A5}$$

Finally, Equations A1, A3, A4, and A5 may be used to obtain population averages of concentration (or other state variables such as nucleotide synthesis rate) according to

$$\langle X(t) \rangle = \left[N_G(t) X_G(t) + \int_0^L n_S(t - t', t) X_S(t', t) dt' / T + N_S X_S(t) \right] N(t)^{-1} \tag{A6}$$

where $X_G(t)$ is the concentration variable computed for a cell always in G, $X_S(t)$ is a similar quantity for a solely S-phase cell, $X_S(t',t)$ is the concentration computed for a cell that ends in S-phase at time t but spent the first portion of its exposure time t' in G-phase, $L = t$ if $0 < t \leq \mu_2 T$ and $L = \mu_2 T$ if $t > \mu_2 T$, and $N(t)$ is the total number of cells at t

$$N(t) = N_G(t) + N_S + \frac{1}{T} \int_0^L n_S(t - t', t) dt'$$

which upon evaluation becomes

$$N(t) = N_G(t) + 2N_0 \times \begin{cases} 2^{t/T + \mu_1 - \mu_2} - 2^{\mu_1 - 1} & \text{(I,II,III)} \\ 2^{\mu_1 - 1} & \text{(IV)} \end{cases}$$

Equation A6 was used to obtain the population-averaged values in Figs. 2 to 7.

REFERENCES

Allegra, C. J., Chabner, B. A., Drake, J. C., Lutz, R., Rodbard, D., and Jolivet, J. (1985) *J. Biol. Chem.* **260,** 9720–9726

Allegra, C. J., Drake, J. C., Jolivet, J., and Chabner, B. A. (1985b) *Proc. Natl. Acad. Sci. U. S. A.* **82,** 4881–4885

Allegra, C. J., Drake, J. C., Jolivet, J., and Chabner, B. A. (1985c) in *Folyl and Folyl Polyglutamates*, Goldman, I. D., ed pp. 348–359, Praeger Publishers, New York

Allegra, C. J., Fine, R. L., Drake, J. C., and Chabner, B. A. (1986) *J. Biol. Chem.* **261,** 6478–6485

Allegra, C. J., Baram, J., Boarman, D., Drake, J. C., and Chabner, B. A. (1987a) *Proc. AACR* **28,** 273

Allegra, C. J., Hoang, K., Yeh, G. C., Drake, J. C., and Baram, J. (1987b) *J. Biol. Chem.* **262,** 13520–13526

Ali Imam, A. M., Crossley, P. H., Jackman, A. L. R., and Little, P. F. (1987) *J. Biol. Chem.* **262,** 7368–7373

Aroesty, J., Lincoln T, Shapiro N., and Boccia, G. (1973) *Math. Biosci.* **17,** 243–300

Ayusawa, D., Shimizu, K, Koyama, H., Kaneda, S., Takeishi, K., and Seno, T. (1986) *J. Mol. Biol.* **190,** 559–567

Baggot, J. E., and Krumdieck, C. L. (1979) *Biochemistry* **18,** 1036–1041

Balinska, M., Nimec, Z., and Galivan, J. (1982) *Arch. Biochem. Biophys.* **216,** 466–476

Baram, J., Chabner, B. A., Drake, J. C., Fitzhugh, A. L., Sholar, P. W., and Allegra, C. J. (1988) *J. Biol. Chem.* **263,** 7105–7111

Baugh, C. M., Krumdieck, C. L., and Nair, M. G. (1973) *Biochem. Biophys. Res. Commun.* **52,** 27–34

Blakeley, R. L. (1969) *The Biochemistry of Folic Acid and Related Pteridines, Frontiers in Biology Series, Vol. 13*, (Neuberger, A., and Tatum, E. L., eds) North-Holland, Amsterdam

Clendeninn, N. J., Drake, J. C., Allegra, C. J., Welch, A. D., and Chabner, B. A. (1985) *Proc. AACR* **26,** 232

Cowan, K. H., and Jolivet, J. (1984) *J. Biol. Chem.* **259,** 10793–10800

Danenberg, P. V., and Danenberg, K. D. (1978) *Biochemistry* **17,** 4018–4024

Dolnick, B. J., and Cheng, Y. (1977) *J. Biol. Chem.* **252,** 7697–7703

Domin, B. A., Grill, S. P., Bastow, K. F., and Cheng, Y. C. (1982) *Mol. Pharmacol.* **21,** 478–482

Drake, J. C., Chabner, B. A., Baram, J., Oliverio, V. T., and Allegra, C. J. (1987a) *Proc. AACR,* **28,** 272

Drake, J. C., Allegra, C. J., Baram, J., Kaufman, B. T., and Chabner, B. A. (1987b) *Biochem. Pharmacol.* **36,** 2416–2417

Fry, D. W., Yalowich, J. C., and Goldman, I. D. (1982) *J. Biol. Chem.* **257,** 1890–1896

Galivan, J. H., Maley, F., and Baugh, C. M. (1976) *Biochem. Biophys. Res. Commun.* **71,** 527–534

Grindey, G. B., Moran, R. G., and Werkheiser, W. C. (1975) in *Drug Design* (Ariens, E., ed) pp. 169–249, Academic Press, New York

IMSL Library Reference Manual, Ed. 9 (1982). International Mathematics and Statistical Libraries Inc, Houston, TX

Jackson, R. C. (1980) *Int. J. Biomed. Comput.* **11,** 197–224

Jackson, R. C. (1986) *Bull. Math. Biol.* **48,** 337–351

Jackson, R. C. (1987) in *New Avenues in Developmental Cancer Chemotherapy*, pp. 3–35, Academic Press, New York

Jackson, R. C., and Harrap, K. R. (1973) *Arch. Biochem. Biophys.* **158,** 827–841

Jackson, R. C., and Harrap, K. R. (1979) *Pharmacol. Ther.* **4,** 245–280

Jacobs, S. A., Derr, C. J., and Johns, D. G. (1977) *Biochem. Pharmacol.* **26,** 2310–2313

Jenh, C-H., Geyer, P. K., and Johnson, L. F. (1985) *Mol. Cell Biol.* **5,** 2527–2532

Jolivet, J., Schilsky, R. L., Bailey, B. D., Drake, J. C., and Chabner, B. A. (1982) *J. Clin. Invest.* **70,** 351–360

Jolivet, J., and Chabner, B. A. (1983) *J. Clin. Invest.* **72,** 773–778

Kennedy, D. G., Clarke, R., Van den Berg, H. W., and Murphy, R. F. (1983) *Biochem. Pharmacol.* **32,** 41–46

Kennedy, D. G., Van den Berg, H. W., Clarke, R., and Murphy, R. F. (1985) *Biochem. Pharmacol.* **34,** 3087–3090

Lorenson, M. Y., Maley, G. F., and Maley, F. (1967) *J. Biol. Chem.* **242,** 3332–3344

MacKenzie, R. E., and Baugh, C. M. (1980) *Biochim. Biophys. Acta* **611,** 187–195

Matthews, R. G., and Baugh, C. M. (1980) *Biochemistry* **19,** 2040–2045

Matthews, R. G., Ross, J., Baugh, C. M., Cook, J. D., and Davis, L. (1982) *Biochemistry* **21,** 1230–1238

Morrison, P. F., and Allegra, C. J. (1987) *Arch. Biochem. Biophys.* **254,** 597–610

Myers, C. E., Young, R. C., and Chabner B. A. (1975) *J. Clin. Invest.* **56,** 1231–1238

Navalgund, L. G., Rossana, C., Muench, A. J., and Johnson, L. F. (1980) *J. Biol. Chem.* **255,** 7386–7390

Nimec, Z., and Galivan, J. (1983) *Arch. Biochem. Biophys.* **226,** 671–680

Poser, R. G., Sirotnak, F. M., and Chello, P. L. (1980) *Biochem. Pharmacol.* **29,** 2701–2704

Rader, J. I., and Huennekens, F. M. (1973)in *The Enzymes*, Vol. 9 (Boyer, P. D., ed) p. 197–223

Reyes, P., and Heidelberger, C. (1965) *Mol. Pharmacol.* **1,** 14–30

Rode, W., Scanlon, K. J., Moroson, B. A., and Bertino, J. R. (1980) *J. Biol. Chem.* **255,** 1305–1311

Rosenblatt, D. S., Whitehead, V. M., Dupont, M. M., Vuchich, M. J., and Vera, J. (1978) *Mol. Pharmacol.* **14,** 210–214

Rubinow, S. I. (1968) *Biophys. J.* **8,** 1055–1073

Santi, D. V., Pogolotti, A. L., James, T. L., Wataya, Y., Ivanetich, K. N., and Lam, S. S. (1976) *ACS Symp. Ser.* **28,** 57–76

Schilsky, R. L., Bailey, B. D., and Chabner, B. A. (1981) *Biochem. Pharmacol.* **30,** 1537–1542

Seither, R. L., and Goldman, I. D. (1988) *Proc. AACR* **29,** 282

Smith, G. K., Mueller, T., Benkovic, P. A., and Benkovic, S. J. (1981) *Biochemistry* **20,** 1241–1245

Tan, L. U. L., Drury, E. J., and MacKenzie, R. E. (1977) *J. Biol. Chem.* **252,** 1117–1122

Werkheiser, W. C. (1971) *Ann. N. Y. Acad. Sci.* **186,** 343–358

Werkheiser, W. C., Grindey, G. B., and Moran, R. G. (1973) *Mol. Pharmacol.* **9,** 320–329

White, J. C. (1979) *J. Biol. Chem.* **254,** 10889–10895

Whitehead, V. M., Perrault, M. M., and Stelcner, S. (1975) *Cancer Res.* **35,** 2985–2990